

UFTP-477/1998  
 YRHI-98-11  
 nucl-th/9806010

# Entropy Production in Collisions of Relativistic Heavy Ions – a signal for Quark-Gluon Plasma phase transition?

M. Reiter<sup>a</sup>, A. Dumitru<sup>b</sup>, J. Brachmann<sup>a</sup>,  
 J.A. Maruhn<sup>a</sup>, H. Stöcker<sup>a</sup>, W. Greiner<sup>a</sup>

<sup>a</sup>Institut für Theoretische Physik der J.W. Goethe-Universität  
 Robert-Mayer Str. 10, Postfach 11 19 32  
 D-60054 Frankfurt a.M., Germany

<sup>b</sup>Physics Department, Yale University  
 P.O. Box 208124, New Haven, Connecticut 06520-8124, USA

June 2, 1998

## Abstract

Entropy production in the compression stage of heavy ion collisions is discussed within three distinct macroscopic models (i.e. generalized RHTA, geometrical overlap model and three-fluid hydrodynamics). We find that within these models  $\sim 80\%$  or more of the experimentally observed final-state entropy is created in the early stage. It is thus likely followed by a nearly isentropic expansion. We employ an equation of state with a first-order phase transition. For low net baryon density, the entropy density exhibits a jump at the phase boundary. However, the excitation function of the specific entropy per net baryon,  $S/A$ , does not reflect this jump. This is due to the fact that for final states (of the compression) in the mixed phase, the baryon density  $\rho_B$  increases with  $\sqrt{s}$ , but not the temperature  $T$ . Calculations within the three-fluid model show that a large fraction of the entropy is produced by nuclear shockwaves in the projectile and target. With increasing beam energy, this fraction of  $S/A$  decreases. At  $\sqrt{s} = 20$  AGeV it is on the order of the entropy of the newly produced particles around midrapidity. Hadron ratios are calculated for the entropy values produced initially at beam energies from 2 to 200 AGeV.

Work supported by BMBF, DFG, GSI and the German Academic Exchange Service (DAAD).

# 1 Introduction

A large amount of entropy can be produced in the initial off-equilibrium stage of energetic nuclear collisions [1]. The subsequent expansion is, on the other hand, often assumed to be isentropic. The linear increase of the pion multiplicity with beam energy observed at the BEVALAC [2] is consistent with a picture [3, 4, 5] where more than 80% of the specific entropy is produced initially. In this scenario the entropy produced during the compression stage is closely linked to the finally observable relative particle yields.

In the present paper, the entropy produced within the compression stage of highly relativistic heavy ion collisions is calculated within three distinct macroscopic models (i.e. generalized RHTA, geometrical overlap model, three-fluid hydrodynamics). Several comparisons of experimental data on relative hadron multiplicities with calculations of chemically equilibrated hadronic gases indicate that the entropy per net baryon at (chemical) freeze-out is on the order of  $S/A = 10 \pm 2.5$  at AGS and  $S/A = 40 \pm 10$  at SPS energies [6, 7, 8, 9]. The microscopic transport model UrQMD also exhibits a chemical composition in the central volume of Au+Au collisions at AGS energies which is compatible with an ideal hadron gas with  $S/A = 12$  [10]. Moreover,  $S/A$  values in this range yield the measured rapidity distributions and transverse momentum spectra of produced hadrons at AGS and SPS, if an isentropic expansion of the hot and dense matter created during the early compression stage is assumed [11].

The question arises, whether and how such a tremendous amount of entropy can indeed be created in the initial stage of the reaction, before local equilibrium is established. If true, this would speak in favour of the picture that the compression stage produces most of the finally observed entropy and that it is followed by a nearly isentropic expansion.

The present study focuses on the excitation function of  $S/A$ , i.e. its dependence on the bombarding energy. In particular, it is interesting to study the behaviour of  $S/A$  for energies where the matter in the central region enters the mixed phase and the pure QGP phase. This analysis reveals whether the produced entropy exhibits an “anomalous” behaviour which could serve as a direct sign of the QGP phase transition [9, 12].

Also, the fraction of entropy produced both by nuclear shockwaves in the projectile and target, on the one hand, and by particle production (and their thermalization) around midrapidity, on the other hand, is studied as a function of bombarding energy within the three-fluid model.

## 2 Models for the compression stage

In this section, the equation of state and the three collective models which will be employed in section 3 to calculate entropy production are described.

### 2.1 The Equation of State

The equation of state (EoS) of the highly excited nuclear matter must be specified in order to determine entropy production in the compression stage. Here, the  $\sigma-\omega$  model [13] is used for

the interactions between the nucleons. The parameters of the Lagrangian are fitted such that the properties of infinite nuclear matter in the ground state are reproduced. The pressure of an ideal pion gas in chemical equilibrium is added to the pressure of the interacting nucleons to account for thermal pion production. Other particles like  $\Delta$ 's and  $\rho$ 's are not included in the EoS, since they probably do not reach thermal and chemical equilibrium in the early stage of the reaction.

At high temperatures or baryon-chemical potentials, a phase transition to the quark-gluon plasma (QGP) is assumed to occur. Here, the MIT bag model is used to calculate the EoS [14] for massless, non-interacting gluons and  $u, d$  quarks. The pressure as a function of temperature  $T$  and quark-chemical potential  $\mu_q$  reads [15]

$$p_{QGP} = \frac{37\pi^2}{90} T^4 + T^2 \mu_q^2 + \frac{1}{2\pi^2} \mu_q^4 - B \quad . \quad (1)$$

A bag parameter of  $B^{1/4} = 235$  MeV is used. The two EoS are matched by Gibbs' conditions of phase equilibrium. The resulting EoS thus exhibits – by construction – a first-order phase transition at a critical temperature (for vanishing  $\rho_B$ ) of  $T_C \approx 170$  MeV. Baryon-, entropy-, and energy-densities can be calculated via the usual thermodynamic relations

$$\begin{aligned} \rho_B &= \left. \frac{\partial p}{\partial \mu_B} \right|_T , \\ s &= \left. \frac{\partial p}{\partial T} \right|_{\mu_B} , \\ \epsilon &= Ts - p + \mu_B \rho_B , \end{aligned} \quad (2)$$

where the baryochemical potential  $\mu_B = 3\mu_q$ . For a more detailed discussion of this EoS refer to [16].

For this EoS, the entropy per net baryon  $s/\rho_B$  exhibits a jump at the phase transition temperature, if  $\rho_B$  is not too large (Fig. 1). However, the excitation function of  $s/\rho_B$  does not show a corresponding jump at a given specific collision energy, as will be discussed in section 3.1.

## 2.2 Geometrical Overlap model

The first model discussed is a simple schematic geometrical overlap model, where the two Lorentz-contracted nuclei are placed on top of each other. Then the following baryon density  $\rho_B$  and energy density  $\epsilon$  are obtained:

$$\rho_B = 2\rho_0 \gamma_{CM} \quad (3)$$

$$\epsilon = \sqrt{s} \rho_0 \gamma_{CM} = \frac{m_N}{2\rho_0} \rho_B^2 \quad . \quad (4)$$

Note that the compression stage is not treated dynamically within this model. Therefore the compression achieved is independent of the EoS. However, the EoS determines the temperature and the entropy density of the compressed matter.

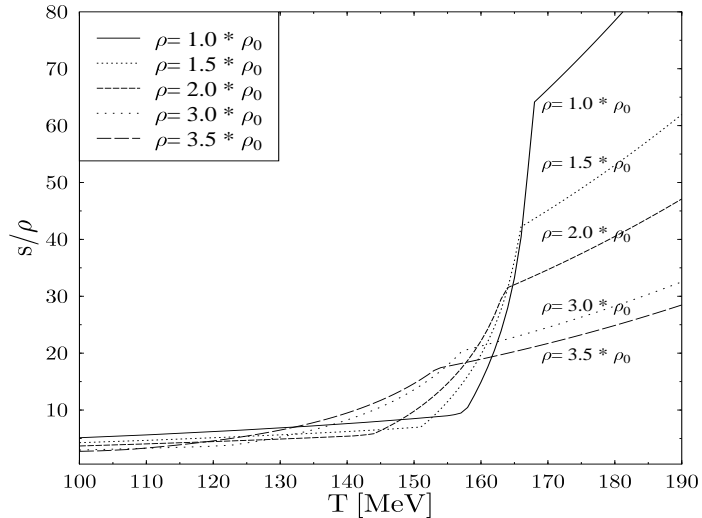


Figure 1: Entropy per net baryon as a function of temperature at various fixed net baryon densities for the EoS used here (see text).

### 2.3 One-fluid hydrodynamics

We now turn to the one-fluid hydrodynamical model, restricting the calculations to an ideal fluid, i.e. viscosity and thermoconductivity effects are neglected [5, 17].

In this model, compression and entropy production occur due to shock discontinuities, or by a combination of shock- and isentropic compressional waves if the compressed matter is thermodynamically anomalous (as e.g. matter in the mixed phase) [16, 18, 19, 20]. The assumption of instantaneous thermalization leads to the maximum energy- and baryon number-deposition in the central region that is consistent with energy-, momentum-, and baryon number-conservation.

As an example, Fig. 2 shows a three-dimensional one-fluid dynamical calculation of the collision of two Au-nuclei at  $\sqrt{s} = 4.9$  AGeV and vanishing impact parameter,  $b = 0$ . The upper panels of Fig. 2 show reaction plane contour plots of the baryon density  $\gamma\rho_B/\rho_0$  in the center of mass frame. Two shockwaves can be clearly observed as high density gradients. They develop in the center and propagate outwards. The entropy produced by these shockwaves is depicted in the lower panel. The entropy per net baryon is computed as

$$\frac{S}{A} = \frac{\int d^3x \gamma s}{\int d^3x \gamma \rho_B} , \quad (5)$$

where  $s$  is the entropy density (cf. eq. 2). The compression stage is finished once the shock fronts reach the back sides of the Lorentz-contracted nuclei. Then an isentropic expansion follows (remember that we assume a non-viscous fluid).

The specific entropy (and also the energy density, the pressure, etc.) of the central region (close to  $x, y, z = 0$ ) in relativistic nucleus-nucleus collisions at  $b = 0$  can also be computed directly by solving the Rankine-Hugoniot-Taub Adiabate (RHTA) equation [16, 17, 18, 20, 21],

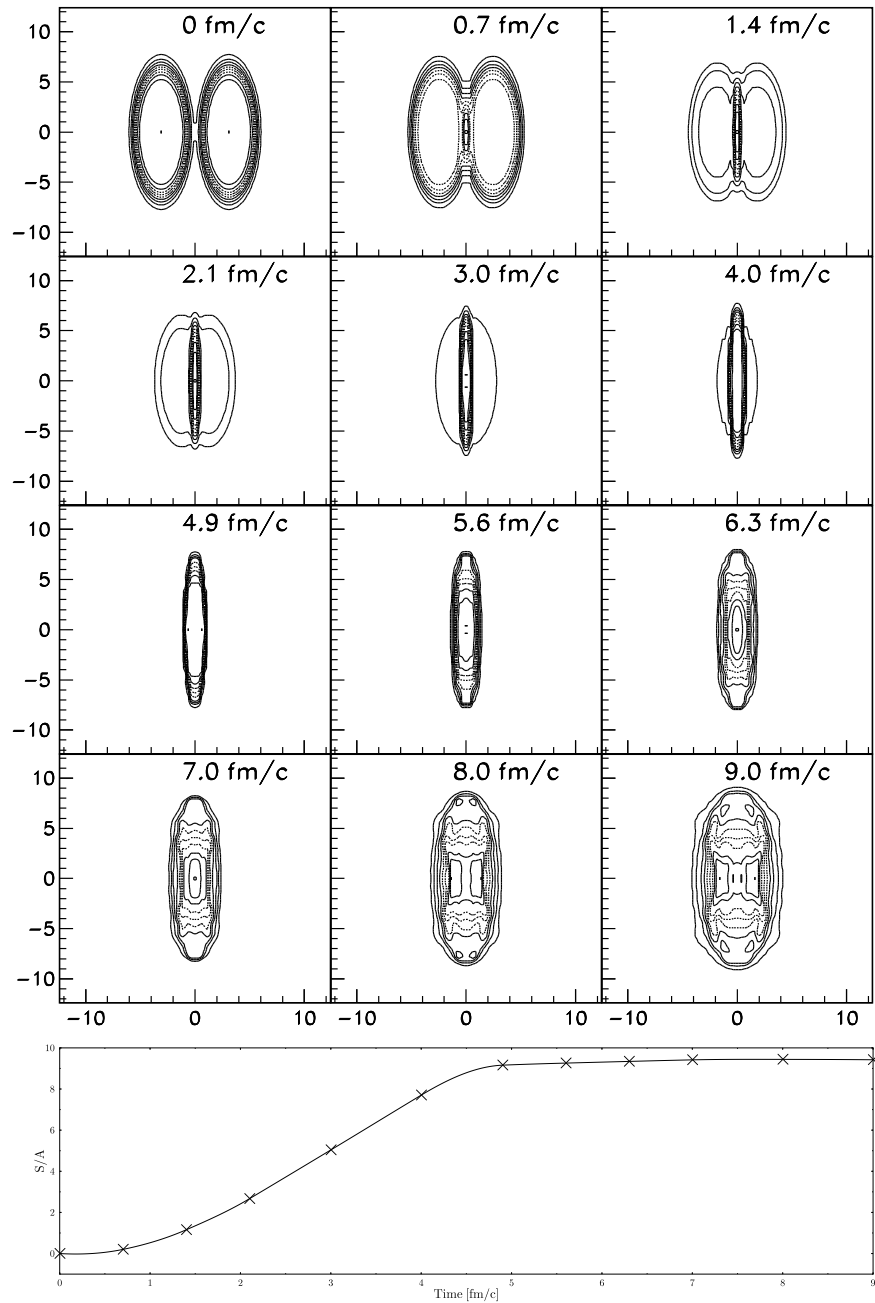


Figure 2: Time evolution of baryon density and  $S/A$  in a 3D one-fluid hydrodynamical calculation of Au+Au at  $\sqrt{s} = 4.9$  AGeV.

thus assuming a one-dimensional “slab-on-slab” collision. The RHTA determines for a given initial state and EoS all shock wave solutions consistent with energy and momentum conservation. Matter in the mixed phase, however, is thermodynamically anomalous and single shock waves become mechanically unstable. Therefore, construction of the generalized RHTA is required [16, 19]. In the generalized RHTA, the unstable shock wave solutions are replaced by a combination of shock waves and an isentropic compression wave. For matter in the pure QGP phase, a single shock becomes again stable. For a given bombarding energy, the generalized RHTA thus determines the thermodynamic properties of the compressed matter (“final” state).  $S/A$  is independent of  $\sqrt{s}$  for all bombarding energies with “final” states in the phase coexistence region (cf. section 3.1), due to the fact that a simple compression wave does not produce any additional entropy.

## 2.4 Three-fluid hydrodynamics

The assumption of instantaneous local thermalization in the one-fluid model prevents the expected partial interpenetration of projectile and target. A more realistic description, allowing for finite mean free path effects, is obtained if two distinct fluids for projectile and target are introduced, which interact locally [22, 23]. These interactions lead to energy and momentum exchange and to a smooth deceleration of the projectile and target fluids. At AGS and SPS energies, it is reasonable to introduce a third fluid that “collects” the produced particles around midrapidity [23, 24]. The model assumes that the fluids are well separated in rapidity (but, of course, not in coordinate space) during the early stage of the reaction. Binary particle collisions increase the overlap of the fluids in momentum space and thus drive the system into (local) mutual kinetic equilibrium. At this point, the various fluids merge into a single fluid [22, 23, 24] and the subsequent expansion proceeds as in the one-fluid hydrodynamical model. The time scale for this kinetic equilibration of the central region was estimated in refs. [24, 25] to be  $\approx 2R/\gamma_{CM}$ . Here the interactions between projectile and target nucleons have been regarded as a sum over incoherent binary nucleon-nucleon scatterings (with cross sections as in vacuum). Since we focus on the early (compressional) stage of the reaction, the one-fluid transition is not discussed here.

The most essential difference to the one-fluid model is that the shock fronts are smeared out considerably, i.e. projectile and target interpenetrate strongly. Consequently, the baryons are less compressed [24, 25] in the three-fluid model. Most of the energy loss of the incoming nucleons results in particle production at midrapidity, i.e. a large part of the energy loss of the nucleons is transferred to the mid-rapidity regime (third fluid) and only a smaller fraction of the energy is deposited in the baryon fluids. The physical mechanism for entropy production is very different in the three-fluid model than in the one-fluid hydrodynamical model, therefore the ratio of the thermal to the compression energy at midrapidity differs from that given by the RHTA equation.

### 3 Results

We now turn to the discussion of entropy production as a function of the bombarding energy for the three different models.

#### 3.1 Excitation function of Specific Entropy

The excitation function of the entropy per (net) baryon is shown in Fig. 3 for the three different models.

1. The geometrical overlap model assumes that energy and baryon density increase as  $\gamma_{CM}^2$  and  $\gamma_{CM}$ , respectively (cf. eqs. (3,4)). As a consequence,  $S/A$  increases continuously with energy. The compressed matter enters the mixed phase at  $\sqrt{s} \approx 2.4$  AGeV with a specific entropy of  $S/A = 4.5$ . Pure QGP matter is produced with  $S/A = 12$  at  $\sqrt{s} \approx 4.6$  AGeV. However, while sweeping through the mixed phase by increasing the bombarding energy,  $\rho_B$  and  $S/A$  increase smoothly, while  $T$  is roughly constant, cf. Fig. 4. Thus, the entropy jump seen in Fig. 1 is not reflected in the  $S/A(\sqrt{s})$  excitation function.

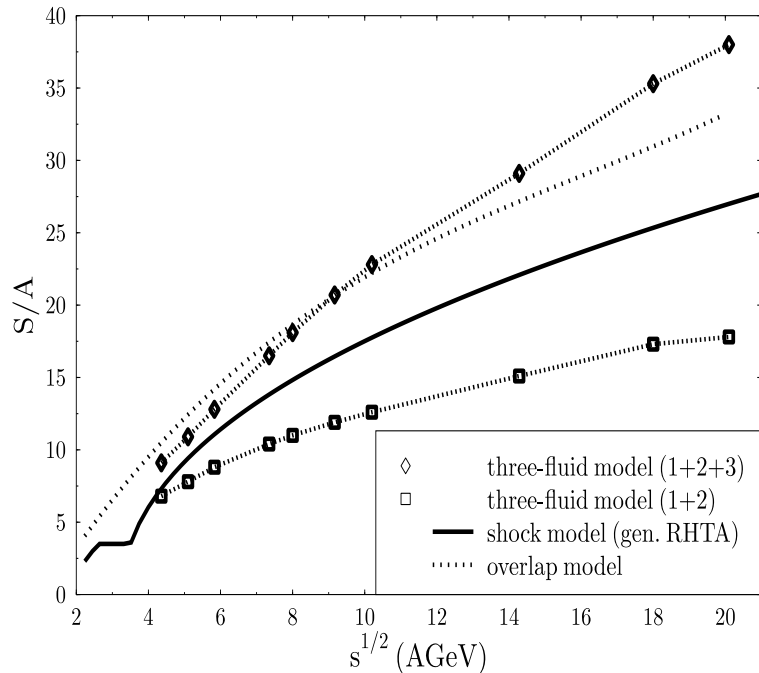


Figure 3: Excitation function of entropy per participating net baryon as calculated within the various models. For the three-fluid model, both the entropy of projectile- and target fluids only (1+2), as well as that of all three fluids (1+2+3) are shown.

2. In contrast, in the shock model (1D RHTA)  $S/A$  first increases with the beam energy and reaches a plateau at  $\sqrt{s} \approx 2.7$  AGeV. At this beam energy the matter enters the

mixed phase. Single shock fronts cease to be the stable solution [16, 18, 19, 20] in this thermodynamically anomalous region. Rather, further compression can only be achieved by a simple compressional wave which, however, conserves the specific entropy. Thus, even when the bombarding energy is increased,  $S/A$  remains constant (isentropic compression) until the anomalous region is left again. Hence, the baryon density increases with energy while the temperature *decreases*, as seen in Fig. 4. In this model,

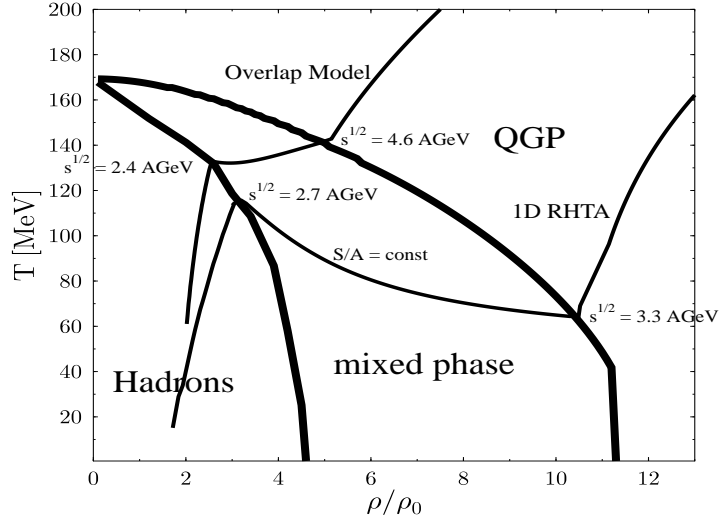


Figure 4: Temperature and (net) baryon density of the compressed matter within the overlap model and the shock model (generalized 1D RHTA), respectively. The phase coexistence region is also indicated.

the participant matter reaches the pure QGP phase at a temperature of  $T = 65$  MeV at  $\sqrt{s} \approx 3.3$  AGeV, which is significantly less than in the overlap model (Fig. 4). The specific entropy then increases monotonically with energy. In the AGS energy range, where a single shock is again stable, we find  $S/A \approx 10$ , in agreement with the numbers obtained from the data analysis on hadron yield ratios [6]. However, the energy density, baryon density, and entropy density are  $\epsilon = 5$  GeV/fm $^3$ ,  $\rho_B = 2.0$  fm $^{-3}$ ,  $s = 19$  fm $^{-3}$ . These values seem unreasonably high at this energy. These huge densities and the very early phase transition to pure QGP matter are due to the assumption of instantaneous stopping and thermalization [22, 23, 24]. At higher energies, the discrepancies become even more pronounced: e.g. for Pb+Pb at SPS,  $\epsilon \approx 50$  GeV/fm $^3$ ,  $\rho_B \approx 6$  fm $^{-3}$ , and  $s \approx 150$  fm $^{-3}$ . These values are close to the analytic expressions  $\epsilon/\epsilon_0 = 4\gamma_{CM}^2 - 3$ ,  $\rho_B/\rho_0 = 4\gamma_{CM} - 3/\gamma_{CM}$  ( $\epsilon_0 = \rho_0 \cdot 923$  MeV = 148 MeV/fm $^3$ ,  $\rho_0 = 0.16$  fm $^{-3}$ ) derived from the RHTA with an ultrarelativistic EoS,  $p = \epsilon/3$ . Because these densities are so huge, the specific entropy is rather low,  $S/A = 25$ . This is in fact significantly below the value  $40 \pm 10$  discussed in [6, 7, 8, 9, 11]. Slightly larger  $S/A$  values are found [26] when the number of degrees of freedom in the QGP is increased, e.g. by including strange quarks. However, at the SPS the compression phase in this model lasts only for  $\approx 1.1$  fm/c (the time when the shockwaves reach the back of the nuclei). Within

this very short time, strange quarks may not reach thermal and chemical equilibrium. In the subsequent expansion, strange quarks (resp. strange hadrons) should be taken into account.

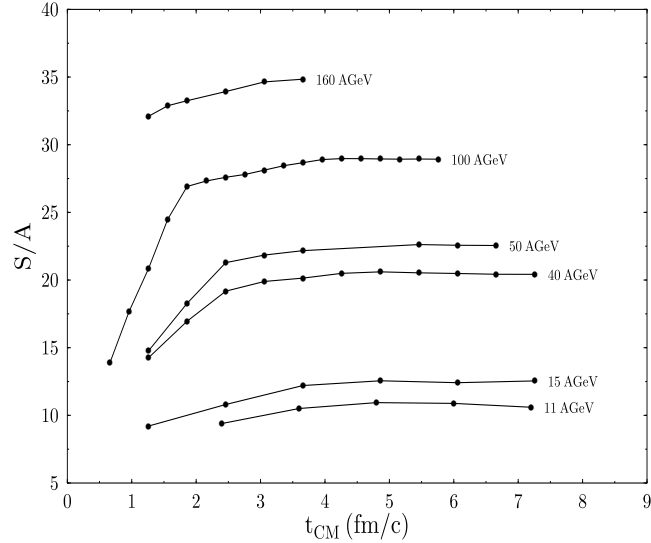


Figure 5: Time evolution of the entropy per net participant baryon for  $Pb + Pb$  reactions at various energies, calculated within the three-fluid model.

3. The three-fluid model predicts the entropy per net participating baryon as a function of CM-time as depicted in Fig. 5. In contrast to our earlier work [24, 25, 27], in this calculation the EoS described in section 2.1 is employed for all three fluids. The third fluid is net baryon free since we assume that the direct baryon transfer to midrapidity is small in the first collisions with large rapidity gap [28]. To calculate  $S/A$  within the three-fluid model a temperature cut of  $T \geq 50$  MeV has been applied to determine participant baryons. This corresponds to a mean transverse momentum of  $\langle p_T \rangle \approx 270$  MeV, roughly in accordance with the  $p_T$  cut employed in [12]. Total entropy and baryon number have then been calculated by summing over all three fluids (resp. projectile and target fluids only for baryon number). Thus:

$$\frac{S}{A} = \frac{\sum_{\text{fluids } 1,2,3} \int d^3x \gamma s \Theta(T - 50 \text{ MeV})}{\sum_{\text{fluids } 1,2} \int d^3x \gamma \rho_B \Theta(T - 50 \text{ MeV})} . \quad (6)$$

At early times,  $t \leq 2R/\gamma_{CM}$ , kinetic equilibrium between the fluids is not established. Thus, summing over the entropy and baryon currents of the individual fluids as in eq. (6) seems physically more meaningful than calculating the entropy and baryon densities from the *total* energy-momentum tensor  $T^{\mu\nu} = T_1^{\mu\nu} + T_2^{\mu\nu} + T_3^{\mu\nu}$  and *total* baryon current  $j^\mu = j_1^\mu + j_2^\mu$  assuming that they are of the form

$$T^{\mu\nu} = (\epsilon + p) u^\mu u^\nu - p g^{\mu\nu} , \quad (7)$$

$$j^\mu = \rho_B u^\mu , \quad (8)$$

as appropriate for a single (ideal) fluid [18]. Fig. 5 shows that  $S/A$  saturates rapidly, and is essentially time independent for later times. This also speaks for the fact that the numerical ‘‘production’’ of entropy is negligible in the present calculations, which focus on the early compression phase of nuclear collisions. Baryon number  $A$  is conserved with an accuracy of  $\sim 0.1\%$  within our model, and the time independency of  $S/A$  shows that this holds also true for the entropy  $S$ , at least for the early stages regarded here.

This plateau value is plotted in Fig. 3 as a function of  $\sqrt{s}$  (diamonds). If one omits the third fluid in calculating the entropy,  $S/A$  saturates similarly. The plateau values reached in this calculation are also depicted in Fig. 3 (squares). One observes that with increasing bombarding energy a larger fraction of the total entropy results from thermalization of the particles produced around mid-rapidity. At SPS, 50% of the total entropy is due to shockwaves in the projectile and target fluids. After  $\sim 2$  fm/ $c$  (measured in the CMS) the central region is in equilibrium [25] and the isentropic one-fluid expansion sets in with  $S/A = 38$  (for  $\sqrt{s} = 20$  AGeV) and  $S/A = 35$  (for  $\sqrt{s} = 18$  AGeV), respectively. This value is 10 units above the one-fluid result quoted above. Consequently, particle ratios involving antibaryons (like  $\bar{N}/\pi$ ,  $\bar{N}/N$ ,  $\bar{\Lambda}/\Lambda$ ) are expected to increase considerably, while meson-meson and baryon-baryon ratios (like  $K/\pi$ ,  $\Lambda/N$ ) do not change very much [26].

Fig. 6 depicts the fluid rapidity density of the entropy within the various fluids. The fluid rapidity is defined as

$$\tanh \eta = v_{\parallel} , \quad (9)$$

where  $v_{\parallel}$  is the fluid velocity component parallel to the beam axis. One observes that the largest contribution to the entropy around  $\eta = 0$  is due to production of a net baryon free QGP within the third fluid. The entropy produced by the shockwaves in the projectile and target is found at  $\eta = \pm 1$ . Note, however, that the entropy distribution in the final state will be *different* from that depicted in Fig. 6. The high pressure gradients lead to reacceleration of the strongly decelerated fluids, i.e. expansion sets in. As shown in [27], the resulting rapidity distribution of the pions, including thermal smearing of the particle momenta, is Gaussian-like and does not exhibit peaks (like  $dS/d\eta$  at  $t_{CM} = 3$  fm/ $c$ , cf. right panel of Fig. 6). In other words, at SPS energy the three-fluid model does not predict boostinvariant initial conditions for the expansion stage. Thus, neither the further evolution of the various rapidity bins nor their final break-up into hadrons (cf. section 3.2) proceeds independently. This is in contrast to the dynamics at collider energies ( $\sqrt{s} \geq 200$  AGeV) as discussed in [29].

### 3.2 Particle Ratios

The initial compression stage is followed by a nearly isentropic expansion, until the freeze-out is reached. This scenario allows to calculate particle ratios as follows. We assume that

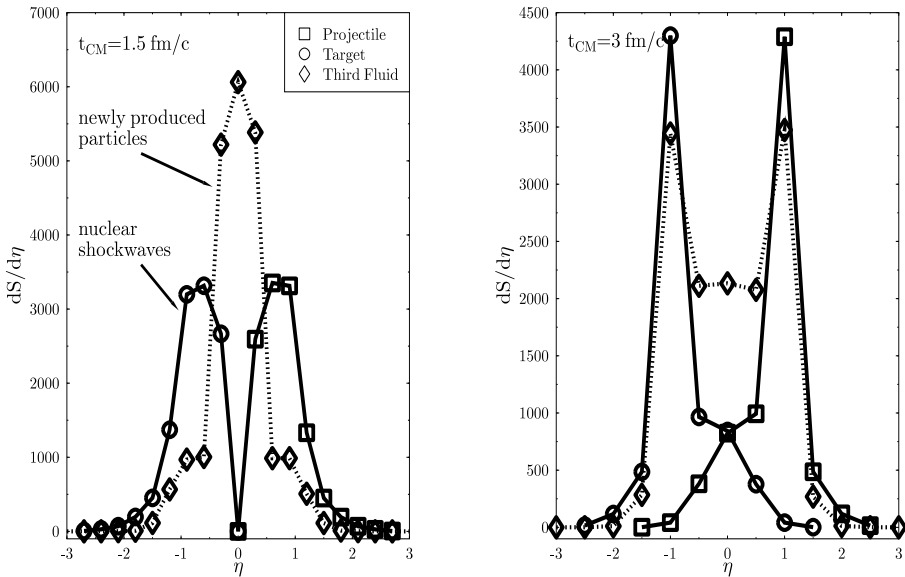


Figure 6: Fluid rapidity distribution of the entropy in Pb+Pb at  $\sqrt{s} = 18$  AGeV as calculated within the three-fluid model at two different CM-times.

at (chemical) freeze-out the net baryon density is  $\rho_B^{fo} = \rho_0/2$  and the net strangeness of the system is zero. The third thermodynamic variable, the specific entropy, is calculated within the three-fluid model, cf. section 3.1. These quantities determine the chemical composition of the fireball – in local thermodynamical equilibrium – unambiguously.

Investigations of hadron ratios at AGS and SPS energies indicate that not only pions and nucleons, but also heavier hadrons (including strange particles), and even clusters like deuterons are close to chemical equilibrium [6, 7, 8, 9] at freeze-out. Therefore an ideal hadron gas model with all known hadrons and resonances up to  $2 \text{ GeV}/c^2$  mass is employed to determine the observable hadron ratios [6]. Feeding from post freeze-out decays of heavy resonances is also taken into account.

We thus implicitly assume that the (fast) compression stage is followed by a rather long expansion stage before (chemical) freeze-out occurs. If this is indeed the case, it is reasonable that the EoS valid within the first  $fm/c$  is different from that at the late freeze-out stage. In principle, the chemical equilibration of the heavier hadrons and resonances can produce additional entropy, which is however neglected in the present analysis.

It has been pointed out that the observed number of pions per net baryon  $n_\pi/n_B$  exhibits an interesting behaviour [12]: For collisions of nuclei in the AGS energy region ( $\sqrt{s} = 5 - 6$  AGeV), the ratio  $n_\pi/n_B$  is smaller than that in  $p + p$  reactions at the same energy (per nucleon). At SPS energies ( $\sqrt{s} = 18 - 20$  AGeV), however, the difference of the ratios is positive. Fig. 7 shows that this can be attributed to the much higher specific entropy at the SPS as compared to the AGS energy. Let us point out again that the excitation function of this difference changes smoothly – it does not exhibit a jump at some specific bombarding

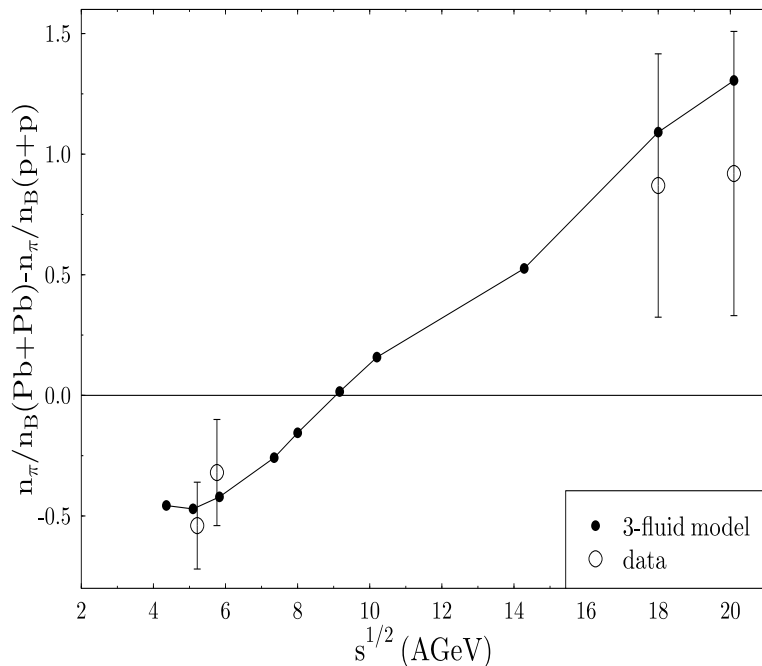


Figure 7: The number of pions per net participant baryon in Pb+Pb minus that ratio for p+p as calculated from the S/A values obtained from the three-fluid model. The feeding due to decays of resonances is taken into account. Experimental data [12] are also shown.

energy (cf. sections 2.1, 3.1) as one might expect from Fig. 1. The average number of pions in  $p + p$  reactions is parametrized as a function of  $\sqrt{s}$  as [30]

$$n_{\pi^+} = -1.7 + 0.84 \ln s + 1.0 s^{-\frac{1}{2}} \quad (10)$$

$$n_{\pi^-} = -2.6 + 0.87 \ln s + 2.7 s^{-\frac{1}{2}} \quad (11)$$

$$n_\pi = \frac{3}{2} (n_{\pi^+} + n_{\pi^-}) . \quad (12)$$

At  $\sqrt{s} \approx 20$  AGeV, about 50% of  $S/A$  are due to thermalization of the energy loss in the third fluid around mid-rapidity (at SPS, this fluid is in fact in the QGP phase with  $\mu_q = \mu_s = 0$ ) and about 50% of  $S/A$  are due to nuclear shockwaves in the projectile and target fluids (which are baryon-rich, but are nevertheless also in the QGP phase). Both contributions therefore are essential to understand the data. As discussed in section 2.4, the three fluids, however, reach kinetic equilibrium later on and merge into a single fluid. Therefore we consider a single fireball as the source of the frozen-out hadrons, rather than letting each of the fluids break up independently.

The hadron ratios at AGS and SPS, cf. Fig. 8, are quite close to the data discussed in the literature [6, 7, 8, 9, 10, 12]. For such a simple<sup>1</sup> estimate of hadron production in nuclear collisions, deviations from the experimental ratios by up to factors of two have to be expected. Nevertheless, it is clear from Fig. 8 that the simultaneous measurement of various hadron ratios, like  $\pi/(B - \bar{B})$ ,  $d/N$  and, in particular,  $\bar{B}/B$  (provided antibaryons also reach chemical equilibrium) allows to determine the produced entropy in the energy range between the AGS and the SPS. In contrast, the  $K/\pi$ -ratio is practically constant.

## 4 Summary and outlook

In the present paper we have calculated the amount of entropy produced in the compression stage of relativistic heavy ion collisions using three different macroscopic models.

The three-fluid model is the only of these models which accounts for (kinetic) non-equilibrium effects between the mutually interacting fluids. Calculations within this model show that the amount of entropy which is due to production of a third fluid (in addition to the projectile and target fluids) of thermalized secondaries around midrapidity can – at higher bombarding energies – exceed the amount of entropy produced by nuclear shockwaves in the projectile and target nuclei. The total specific entropy  $S/A$  produced within this model is consistent with the  $S/A$  values extracted from data using relative particle yields from equilibrated hadron gases. We find, e.g.,  $S/A = 11$  for AGS and  $S/A = 38$  for SPS energies.

---

<sup>1</sup>We neglect e.g. that some hadron species might not reach their chemical equilibrium abundance or decouple earlier (at higher  $\rho_B^{fo}$ ) than others. We also do not discuss here the rapidity dependence of hadron ratios (cf. e.g. [31] for a calculation within the microscopic transport model UrQMD) to study whether the various contributions to  $dS/d\eta$ , as depicted in Fig. 6, can be disentangled. This requires the one-fluid solution in that part of the forward light-cone between the freeze-out hypersurface and the hypersurface where local kinetic equilibrium between the fluids is established. Such a calculation is out of the scope of the present work.

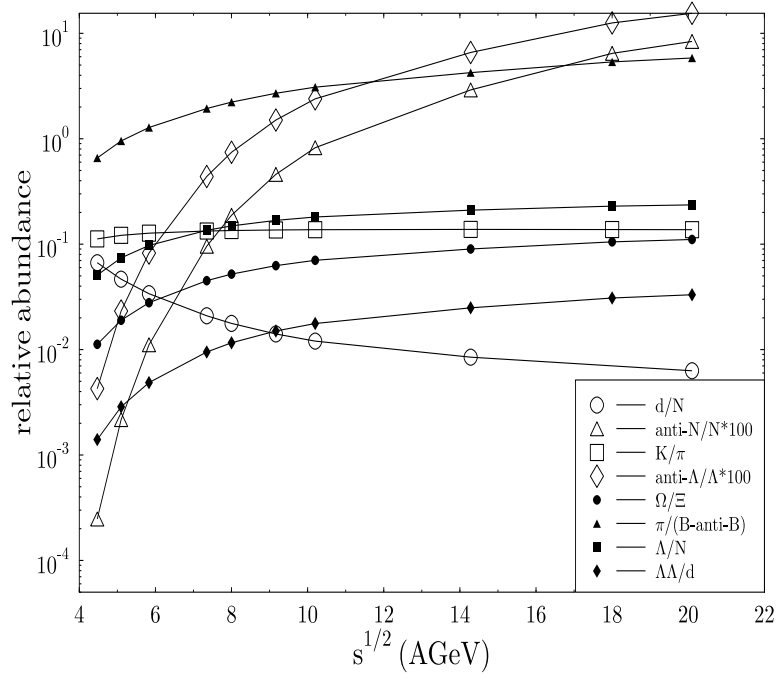


Figure 8: The excitation function of various particle ratios as calculated from the S/A values obtained from the three-fluid model. Feeding due to decays of resonances is taken into account.

The present calculations therefore support the picture that most of the entropy production in relativistic heavy ion collisions occurs in the early compression stage. Then a (nearly) isentropic expansion follows.

The excitation function of the specific entropy  $S/A(\sqrt{s})$  does not exhibit any threshold signatures of the phase transition to the QGP, which is included in the EoS. Nevertheless, the phase transition might still be visible in the excitation functions of other observables, like e.g. directed in-plane flow.

The predicted particle yields exhibit a smooth excitation function, too. Simultaneous measurement of various hadron ratios allows to determine the amount of entropy produced in relativistic heavy ion collisions.

Future work will also consider the rapidity and transverse momentum spectra of various particles at freeze-out. A different EoS will be used during the expansion stage in order to account for the chemical equilibration of additional particle species. The evolution of the rapidity density of the entropy until freeze-out will be studied.

## 5 Acknowledgements

We are indebted to M. Ga  dzicki, M.I. Gorenstein, D.H. Rischke, D. R  hrich and R. Stock for helpful discussions. A. Dumitru acknowledges a postdoctoral fellowship granted by the German Academic Exchange Service (DAAD).

## References

- [1] W. Scheid, H. Müller, W. Greiner: Phys. Rev. Lett. 32 (1974) 741;  
M.I. Sobel, P.J. Siemens, J.P. Bondorf, H.A. Bethe: Nucl. Phys. A251 (1975) 502;  
L.P. Csernai, J.I. Kapusta: Phys. Rep. 131 (1986) 223;  
H. Stöcker, W. Greiner: Phys. Rep. 137 (1986) 277;  
R.B. Clare, D. Strottman: Phys. Rep. 141 (1986) 177
- [2] J. Harris et al.: Phys. Lett. B153 (1985) 377;  
R. Stock: Phys. Rep. 135 (1986) 259
- [3] H. Stöcker, W. Greiner, W. Scheid: Z. Phys. A286 (1978) 121;  
H. Stöcker: J. Phys. G10 (1984) L111;  
D. Hahn, H. Stöcker: Nucl. Phys. A476 (1988) 718
- [4] G. Bertsch, J. Cugnon: Phys. Rev. C24 (1981) 2514
- [5] I.M. Mishustin, F. Myhrer, P.J. Siemens: Phys. Lett. B95 (1980) 361;  
L.P. Csernai, H.W. Barz: Z. Phys. A296 (1980) 173;  
J. Kapusta: Phys. Rev. C24 (1981) 2545
- [6] P. Braun-Munzinger, J. Stachel, J.P. Wessels, N. Xu: Phys. Lett. B344 (1995) 43; Phys. Lett. B365 (1996) 1
- [7] C. Spieles, H. Stöcker, C. Greiner: Eur. Phys. J. C2 (1998) 351;  
A. Dumitru, C. Spieles, H. Stöcker, C. Greiner: Phys. Rev. C56 (1997) 2202
- [8] J. Sollfrank: J.Phys. G23 (1997) 1903-1919 and references therein
- [9] J. Letessier, A. Tounsi, U. Heinz, J. Sollfrank, J. Rafelski: Phys. Rev. Lett. 70 (1993) 3530;  
E. Suhonen, J. Cleymans, K. Redlich, H. Satz: hep-ph/9310345;  
J. Cleymans, D. Elliott, H. Satz, R.L. Thews: Z. Phys. C74 (1997) 319;  
G.D. Yen, M.I. Gorenstein, W. Greiner, S.N. Yang: Phys. Rev. C56 (1997) 2210
- [10] L.V. Bravina et al.: nucl-th/9804008
- [11] J. Sollfrank, P. Huovinen, M. Kataja, P.V. Ruuskanen, M. Prakash, R. Venugopalan: Phys. Rev. C55 (1997) 392;  
C.M. Hung, E. Shuryak: Phys. Rev. C57 (1998) 1891
- [12] M. Gazdzicki, D. Röhricht: Z. Phys. C65 (1995) 215;  
J. Günther: PhD Thesis, Univ. Frankfurt, 1997
- [13] M.I. Gorenstein, D.H. Rischke, H. Stöcker, W. Greiner: J. Phys. G19 (1993) L69
- [14] A. Chodos, R.L. Jaffe, K. Johnson, C.B. Thorn, V. Weisskopf: Phys. Rev. D9 (1974) 3471

- [15] S.A. Chin: Phys. Lett. B78 (1978) 552;  
 J. Kapusta: Nucl. Phys. B148 (1979) 461;  
 E.V. Shuryak: Phys. Rep. 61 (1980) 71;  
 J. Cleymans, R.V. Gavai, E. Suhonen: Phys. Rep. 130 (1986) 217
- [16] D.H. Rischke, Y. Pürsün, J.A. Maruhn: Nucl. Phys. A595 (1995) 383
- [17] P. Danielewicz: Phys. Lett. B146 (1984) 168
- [18] L.D. Landau, E.M. Lifshitz: “Fluid Mechanics”, Pergamon Press, New York, 1959
- [19] K.A. Bugaev, M.I. Gorenstein, V.I. Zhdanov: Z. Phys. C39 (1988) 365;  
 K.A. Bugaev, M.I. Gorenstein, B. Kämpfer, V.I. Zhdanov: Phys. Rev. D40 (1989) 2903;  
 K.A. Bugaev, M.I. Gorenstein, D.H. Rischke: Phys. Lett. B255 (1991) 18;  
 D.H. Rischke, Y. Pürsün, J.A. Maruhn, H. Stöcker, W. Greiner: Heavy Ion Phys. 1 (1995) 309
- [20] J. Hofmann, H. Stöcker, U. Heinz, W. Scheid, W. Greiner: Phys. Rev. Lett. 36 (1976) 88
- [21] A.M. Taub: Phys. Rev. 74 (1948) 328;  
 H.G. Baumgardt et al.: Z. Phys. A237 (1975) 359;  
 J.R. Nix: Prog. Part. Nucl. Phys. 2 (1979) 237;  
 H. Stöcker, M. Gyulassy, J. Boguta: Phys. Lett. B103 (1981) 269
- [22] A.A. Amsden, A.S. Goldhaber, F.H. Harlow, J.R. Nix: Phys. Rev. C17 (1978) 2080;  
 L.P. Csernai, I. Lovas, J.A. Maruhn, A. Rosenhauer, J. Zimányi, W. Greiner: Phys. Rev. C26 (1982) 149;  
 H.W. Barz, B. Kämpfer, L.P. Csernai, B. Lukacs: Nucl. Phys. A465 (1987) 743;  
 H.W. Barz, B. Kämpfer: Phys. Lett. B206 (1988) 399
- [23] I.N. Mishustin, V.N. Russkikh, L.M. Satarov: Sov. J. Nucl. Phys. 48 (1988) 454; Nucl. Phys. A494 (1989) 595;  
 L.M. Satarov: Sov. J. Nucl. Phys. 52 (1990) 264;  
 I.N. Mishustin, L.M. Satarov, V.N. Russkikh: in “Relativistic Heavy Ion Physics” (eds. D. Strottman and L.P. Csernai), vol. 1, World Scientific (Singapore), 1991, p.179 and Sov. J. Nucl. Phys. 54 (1991) 459
- [24] J. Brachmann, A. Dumitru, J.A. Maruhn, H. Stöcker, W. Greiner, D.H. Rischke: Nucl. Phys. A619 (1997) 391
- [25] A. Dumitru, J. Brachmann, M. Bleicher, J.A. Maruhn, H. Stöcker, W. Greiner: Heavy Ion Phys. 5 (1997) 357
- [26] D.H. Rischke, B.L. Friman, B.M. Waldhauser, H. Stöcker, W. Greiner: Phys. Rev. D41 (1990) 111

- [27] A. Dumitru, U. Katscher, J.A. Maruhn, H. Stöcker, W. Greiner, D.H. Rischke: Phys. Rev. C51 (1995) 2166
- [28] V. Blobel et al.: Nucl. Phys. B69 (1974) 454
- [29] R. Anishetty, P. Koehler, L. McLerran: Phys. Rev. D22 (1980) 2793;  
J.D. Bjorken: Phys. Rev. D27 (1983) 140
- [30] M. Antinucci, A. Bertin, P. Capiluppi, M. d'Agostino-Bruno et al.: Lett. Nuov. Cim. 6 (1973) 121
- [31] S.A. Bass et al.: nucl-th/9711032